Research Square

Preprints are preliminary reports that have not undergone peer review.
They should not be considered conclusive, used to inform clinical practice,
or referenced by the media as validated information.

Engineering phosphate-controlled poly(3-hydroxybutyrate) production in Vibrio natriegens from renewable feedstocks

Roland J Politan
The University of Western Australia
Joshua Z Wong
The University of Western Australia
Kathryn M Morris
The University of Western Australia
Bassey F Bassey
The University of Western Australia
Ben RK Roller
University of Vienna
Gavin R Flematti
The University of Western Australia
Simona Della Valle
The University of Western Australia
Georg Fritz
georg.fritz@uwa.edu.au
The University of Western Australia

Research Article

Keywords: Vibrio natriegens, poly-3-hydroxybutyrate, phosphate regulation, acetate, metabolic engineering, bioproduction

Posted Date: October 7th, 2026

DOI: https://doi.org/10.21203/rs.3.rs-10980126/v1

License: This work is licensed under a Creative Commons Attribution 4.0 International License.
Read Full License

Additional Declarations: Competing interest reported. Woodside Energy Ltd co-funded the Australian Research Council Linkage Project under which this work was carried out. The two colleagues thanked in the Acknowledgements for input and discussions, Dr Jitendra Joshi and Dr Sahil Garg, were affiliated with Woodside Energy Ltd during this work. Woodside reviewed the manuscript before submission, and the authors retained full control over its content and over the decision to submit. No author is employed by, or holds a financial interest in, Woodside Energy Ltd. The authors have no other financial or non-financial interests to disclose.

Abstract

Poly(3-hydroxybutyrate) (PHB) is a biodegradable polyester and a leading candidate to replace petrochemical plastics, but high production costs and the reliance on chemical inducers or tightly controlled nutrient feeding hinder its scale-up. Here we show that the fast-growing marine bacterium *Vibrio natriegens* accumulates PHB in response to phosphate limitation, and we exploit this native response to build an autonomous, inducer-free two-stage process. Using a luminescence biosensor of the native *phaBAPC* operon, we found that its promoter is induced by phosphate starvation, but not nitrogen, depletion, a previously unreported regulatory pattern for a *Vibrio* species. Because the cells deplete phosphate as they grow, the switch from growth to PHB production is dynamic and self-actuating, and requires no chemical inducer or engineered regulatory circuit. Integrating additional *phaBAPC* copies into competing biosynthetic and neutral loci, which simultaneously deletes those loci, led to a three-fold increase in PHB titer using acetate as sole carbon source. Process optimization towards a residual-phosphate induction regime further improved production, and a kinetic model predicted the initial phosphate concentration maximizing volumetric titer; validation near this optimum yielded 0.123 g/L PHB in shake flask cultures. Under low-phosphate conditions, the strain accumulated up to 69.1% PHB per cell dry weight from acetate alone, without complex nutrient supplementation. Phosphate starvation also drove PHB synthesis from glycerol, succinate and three sugars, which enter central metabolism at different points from acetate. The switch therefore works wherever carbon enters metabolism, and the feedstock can be chosen on cost and sustainability grounds. Together, these results demonstrate phosphate depletion as an autonomous trigger for sustainable two-stage PHB production in *V. natriegens*.

Key points

• Phosphate limitation triggers inducer-free PHB switch in

• Extra chromosomal copies tripled PHB titer from acetate

• Strain reached 69.1% PHB/cell dry weight without complex nutrient supplementation

Introduction

Plastic pollution has become one of the defining environmental challenges of our time. Since large-scale manufacturing began in the 1950s, synthetic plastics have become indispensable across packaging, agriculture, medicine, and transport, with annual primary production now reaching roughly 414 million tons (Geyer et al., 2017; “Plastics – the fast Facts 2024 • Plastics Europe,” 2004). The very durability that makes these materials useful renders them persistent pollutants, and growing concern over their environmental burden has intensified the search for biodegradable, bio-based replacements (Rosenboom et al., 2022). Among the candidates, poly(3-hydroxybutyrate) (PHB) is one of the most attractive: a microbial polyester accumulated by many bacteria as an intracellular carbon and energy store, it offers mechanical properties comparable to commodity plastics such as polypropylene and

polyethylene, degrades fully in soil and marine environments, and, depending on feedstock and process, can be produced with a substantially lower greenhouse-gas footprint than petrochemical plastics (Chen et al., 2024). Its widespread adoption is predominantly limited by cost, which is set by two levers: the carbon feedstock that fuels microbial polymer production, and the bioprocess framework (Choi and Lee, 1999; Koller and Braunegg, 2018).

The feedstock is the single largest contributor to production cost, with the carbon source alone estimated to account for up to half of the total, and it is also a key determinant of the process' carbon intensity (Choi and Lee, 1999). PHB is most often produced from refined sugars such as glucose and sucrose, which sustain high product titers but compete with food crops for arable land, water, and fertilizers, thereby eroding the environmental case for the bioplastic. Acetate is an attractive alternative: a non-food, two-carbon (C_2) organic compound that can be generated renewably from carbon dioxide (CO_2), syngas, and industrial off-gases, either biologically by acetogenesis through the Wood-Ljungdahl pathway (Groher and Weuster-Botz, 2016; Moreira et al., 2023) or electrochemically by the reduction of CO_2 or carbon monoxide (CO), with increasingly high Faradaic efficiency (Jin et al., 2023). Coupling PHB synthesis to acetate consumption thus embeds the product in a circular carbon economy, and several bacteria already produce PHB efficiently from this substrate, including *Cupriavidus necator*, which reaches titers of 58.5 g/L on acetate in optimized fed-batch (Vlaeminck et al., 2022), and the halophile *Salinivibrio* sp. (Tao et al., 2022; Zhang et al., 2026).

Beyond the use of low-cost, next-generation feedstocks, bioprocess optimization is also key to delivering economically sustainable PHB production at scale. As a bacterial carbon storage compound, PHB is typically accumulated in response to environmental triggers. Namely, intracellular PHB stores are synthesized when a nutrient other than carbon becomes growth-limiting while carbon remains in excess (Anderson and Dawes, 1990). Depending on the organism, that limiting nutrient may be nitrogen, phosphate, or oxygen (Anderson and Dawes, 1990; Babel and Steinbüchel, 2003).

This physiological response can be harnessed in a bioprocess context to temporally separate growth and production: high titer and yield can be attained by first building dense biomass under nutrient-replete conditions and then shifting cells into a production phase in which carbon flux is redirected from growth into storage (Anderson and Dawes, 1990; Kadouri et al., 2005). This two-stage design underpins most high-yielding PHB fermentations. The biosynthetic genes are either turned on with a chemical inducer, or the culture is constrained into production by carefully timed nutrient feeding (Riedel et al., 2012). The former scales poorly, as common small molecule inducers such as isopropyl-beta-D-thiogalactopyranoside are costly at production scale and can burden the host (Shariati et al., 2021). In contrast, tailored nutrient supply offers a simpler and more feasible path to scalable PHB production by implementing an autonomous switch between fermentation stages: biomass accumulation draws down nutrient concentrations, and its depletion forces the culture into production with no exogenous intervention.

Establishing such a process requires knowledge of which environmental conditions trigger PHB synthesis in a particular host organism, how that response is orchestrated, and whether it can be further optimized through targeted metabolic or process interventions. For non-model bacteria now emerging as industrial chassis, this physiological knowledge is often lacking, as their native capacity for PHB production has not been systematically characterized.

Vibrio natriegens is one such emerging chassis, and is exceptionally well-suited for next-generation biomanufacturing (Della Valle et al., 2025; Hädrich et al., 2024; Hoff et al., 2020). This non-pathogenic marine gamma-proteobacterium is among the fastest-growing bacteria known, with a doubling time below ten minutes (Eagon, 1961), and unlike its pathogenic relatives it carries none of the canonical *Vibrio* toxins (Weinstock et al., 2016). Its native halotolerance allows fermentation in saline and seawater-based media (Li et al., 2023), conserving freshwater and enabling non-sterile operation, and a rapidly expanding genetic toolkit now makes it readily engineerable (Dalia et al., 2017; Faber et al., 2025; Stukenberg et al., 2024, 2021; Tschirhart et al., 2019). Crucially, *V. natriegens* natively encodes the *phaBAPC* operon, which comprises the PHB biosynthetic genes together with a phasin, and accumulates PHB from a range of substrates including acetate, as we and others have shown (Faber et al., n.d.; Li et al., 2023; Politan et al., 2025). It therefore unites in one organism the capacity for sustainable feedstock utilization and the genetic tractability needed to elucidate and engineer an autonomous production process. However, the regulatory circuits that govern native PHB accumulation in *V. natriegens*, and whether these can be exploited to build an efficient, self-triggering bioprocess, is yet to be characterized.

Here, we close and exploit this gap to engineer autonomous, inducer-free PHB production in *V. natriegens*. We first build a transcriptional biosensor of the native *phaBAPC* operon and screen nutrient limitations to identify the environmental signal that triggers PHB biosynthesis. We then harness this signal to drive two-stage PHB production from acetate, relying solely on the cells' own consumption of the limiting nutrient, rather than any exogenous chemical inducer or engineered inducible circuit, to dynamically switch the culture from growth into production. To raise output, we engineer the strain by integrating additional chromosomal copies of the *phaBAPC* operon, and we develop a kinetic model that renders the autonomous switch predictable and allows the nutrient regime to be optimized. Together, these results establish, to our knowledge, the first *V. natriegens*-based PHB production process in which a native nutrient-depletion response is used directly as a self-actuating switch, advancing both of our knowledge of this organism and its implementation as a host for sustainable biomanufacturing.

Methods

Bacterial strains, media, and growth conditions

All strains used in this study are listed in Table S3. *V. natriegens* was cultured in LBv2 medium for plasmid transformation and genome-engineering procedures (see below). For plate-reader and shake-flask experiments, *V. natriegens* was propagated in modified "MOPS2" minimal medium (Faber et al., 2025; Politan et al., 2025), which permits independent titration of nitrogen and phosphate because it

does not use a phosphate buffering system. Unless stated otherwise, liquid cultures were grown at 37°C with shaking at 220 rpm. Unless indicated otherwise, a standard preculture was prepared by streaking cells from cryostock, growing them overnight (15–16 h) in MOPS2 supplemented with 60.5 mM sodium acetate (NaOAc), diluting to OD_{600} ~0.01 in fresh medium, and growing to mid-exponential phase (OD_{600} 0.4–0.8). For plasmid-based experiments, kanamycin and chloramphenicol were added to final concentrations of 200 µg/mL and 4 µg/mL, respectively.

Plasmid assembly and biosensor design

Oligonucleotides and plasmids used in this study are listed in Tables S4-S6. The P_{pha} biosensor was designed to include the P_{pha}-promoter region (592 bp upstream of the *phaB*, CDS based on the prediction by (LaFleur et al., 2022), Fig. S1) driving expression of a luciferase operon (Stukenberg et al., 2021). The promoter sequence was amplified from the *V. natriegens* ATCC14048 Δ*dns* ΔVNP1 + 2 genome with Q5 polymerase using the forward primer (AAAACGTCTCGCTCGGGAGCATCAATGTTTAATCAGCGCGTC) and reverse primer (AAAACGTCTCCCTCACATTATTATGACGACTCCATTCTTTATCGGAA), verified by gel electrophoresis, and purified using the EZNA Cycle Pure Kit (Omega Bio-tek) according to the manufacturer's instructions. The purified amplicon was cloned into the entry vector pMC_V_01_Part entry sfGFP from the Marburg Collection (Stukenberg et al., 2021) and transformed into *E. coli* DH5α. The resulting plasmid was verified with colony PCR, and plasmid from correct colonies extracted with the EZNA Plasmid DNA Mini Kit (Omega Bio-tek). The biosensor was then assembled via Golden Gate assembly with parts listed in Table S4, following a published method (Stukenberg et al., 2021), and plasmid extraction was repeated.

Generation of V. natriegens mutants

Strain engineering was performed with the NT-CRISPR protocol according to previous studies with oligonucleotides listed in Table S6 (Faber et al., 2025; Stukenberg et al., 2022). The NT-CRISPR plasmids were those developed for the Vnat Collection (Faber et al., 2025). The tDNA plasmids (listed in Table S4) were assembled by Golden Gate assembly using dropout parts generated in a previous study (Faber et al., 2025).

In silico identification of candidate depolymerase genes

Profile hidden Markov models (HMM) for all homologous families of PHA depolymerases were obtained from the PHA Depolymerase Engineering Database (http://www.ded.uni-stuttgart.de/) (Knoll et al., 2009). The GenomeNet MOTIF Search tool (https://www.genome.jp/tools/motif/MOTIF2.html) (Kanehisa, 2002) was used to search these profile HMMs against the KEGG GENES sequence database for *V. natriegens* (organism code: vna) to identify putative depolymerase genes. Candidate genes that did not encode an α/β-hydrolase domain were excluded from further analysis, as this domain is known to be common to all PHA depolymerases (Knoll et al., 2009).

Plate reader (biosensor) assays

Bacterial growth and reporter kinetics were monitored using a BioTek Synergy HTX microplate reader. For the experiment in Fig. 1, V. *natriegens* cells were pre-adapted by growth in MOPS2 with 60.5 mM NaOAc to mid-exponential phase (OD_{600} = 0.4–0.8), then diluted into fresh medium to an initial OD_{600} of 0.01 in a 96-well black flat-bottom plate containing varying levels of phosphate (Pi) and nitrogen (N), at a final volume of 100 µL per well. To limit evaporation, ddH_2O was added to inter-well spaces and the plate was sealed with parafilm. The plate was incubated at 37°C with orbital shaking at 425 cpm, and the luminescence signal was measured at 10 minutes interval. Blanks were subtracted using the mean of three wells containing fresh media, and the data were computationally adjusted to start at OD_{600} = 0.01. Assays were performed with biological duplicates on two separate days to confirm reproducibility.

PHB production in shake flasks under phosphate starvation

PHB production was induced by phosphate starvation using one of three regimes, all starting from the standard acetate-grown preculture described above and incubated at 37°C, 220 rpm in baffled flasks filled to 20% of their nominal volume (e.g. 20 mL in a 100 mL flask, or 200 mL in a 1 L flask) unless noted.

Wash-based protocol (complete phosphate withdrawal; Figs. 1, 2, S2*).* Mid-exponential cells (OD_{600} 0.4–0.8, 4 mL volume) were centrifuged (5,000 × g, 1 min), washed with 0.5 volumes of phosphate-deplete MOPS2, and resuspended in 5 volumes of the same phosphate-deplete medium.

*Defined-phosphate protocol for kinetic modelling (*Fig. 3*).* Precultures of strain 5X were prepared from single colonies in MOPS2 with 60.5 mM NaOAc at the respective defined initial phosphate concentration (see Results) and grown to OD_{600} > 0.4. To obtain the large sample volumes needed for precise PHB quantification at the low biomass yields on acetate, a batch-cultivation approach was used: for each timepoint, independent triplicate 50 mL cultures (in 250 mL baffled flasks) were inoculated from a common preculture to an initial OD_{600} of 0.01 and harvested in their entirety at the designated timepoint, rather than repeatedly sampling a single culture.

Dilution-based protocol (residual phosphate; Fig. 4*).* When precultures reached OD_{600} 0.4–0.5, they were spun down at 5,000x g for 1 minute in a 15 mL falcon tube. The supernatant was decanted, and the pellet was resuspended in the residual ~ 100 µL prior to a 1:200 dilution (20 mL final volume) directly into phosphate-free MOPS2 containing the respective carbon source, without a wash step. This carries over a residual phosphate concentration of approximately 2.5 µM (1:200 of the ~ 0.5 mM estimated to remain in the preculture at this OD), imposing a milder phosphate limitation than the wash-based protocol. For the carbon-source screen, media contained carbon-equimolar concentrations of sodium acetate, glycerol, disodium succinate, glucose, fructose, or sucrose, and non-sodium carbon sources were supplemented with 60.5 mM NaCl.

Carbon starvation for depolymerase verification

Depolymerase candidate mutants were assessed in a tandem starvation assay. Mutants were grown in MOPS2 and subjected to phosphate starvation for PHB accumulation as described above. After 24 h of phosphate starvation, cells were centrifuged (5,000 × g, 1 min) and the supernatant decanted. The cells were resuspended in 20 mL of phosphate-replete MOPS2 without any carbon source to impose carbon starvation and incubated at 37°C for a further 24 h. Timepoint samples were collected and fixed for BODIPY quantification as described below.

Flow cytometry

Samples were prepared as described previously (Politan et al., 2025). Briefly, cold formaldehyde was added to the culture to a final concentration of 4% and incubated at 4°C for 1 h. Cells were washed twice (centrifugation at 10,000 × g for 1 min, supernatant removal, and resuspension in 0.5 volumes of fresh medium), then resuspended in the same medium and stored at 4°C until analysis, typically within 7 days. Fixed samples were diluted 1:200 to ~ 10^4–10^5 cfu/mL in 0.5× PBS with 5 mM EDTA, then double-stained with BODIPY (Sigma-Aldrich) and Syto62 (Thermo Fisher) at final concentrations of 2 µM and 1 µM to visualize intracellular PHB and DNA, respectively. Stained cells were incubated at 37°C for 15 min. Data were acquired on a FACSCanto (BD Biosciences) using 1× PBS as sheath fluid, with a limit of 10,000 events. BODIPY and Syto62 signals were detected at 488/530 ± 30 nm and 633/660 ± 20 nm, respectively; the forward-scatter, side-scatter, BODIPY, and Syto62 voltages were set to 450, 430, 420, and 603, respectively. Data were analyzed and visualized in R using the FlowCore and openCyto packages, gating on Syto62-positive events to distinguish bacteria from debris.

Analytical methods

For extracellular acetate, culture samples were centrifuged (10,000 × g, 1 min) and the supernatant diluted 1:10 in ddH_2O before HPLC analysis as described below. Volumetric PHB titer was determined by acidolysis and quantified as crotonic acid. Briefly, 10 mL of sample (or 50 mL for the modeling experiment) was centrifuged (7,197 × g, 5 min); the pellet was resuspended in 2% (w/v) sodium chloride, transferred to a pre-weighed glass tube, and dried for 48 h at 60°C. The cell dry weight (CDW) was obtained from the mass difference after subtracting the sodium chloride added. Acidolysis was performed by adding 1 mL of 98% sulfuric acid to the pellet and incubating for 1 h in boiling water; the reaction was cooled to room temperature, diluted with 4 volumes of ddH_2O on ice, and then diluted a further 10-fold in ddH_2O. Extracellular phosphate was quantified with the malachite green phosphate assay kit (Sigma-Aldrich MAK307) following the supplied protocol. When required, samples were diluted 1:10 in ddH_2O to stay within the reported range of the kit (2-150 µM). Residual biomass was calculated by subtracting the measured PHB from the CDW.

Acetate, crotonic acid, and sugars were quantified by high-pressure liquid chromatography (HPLC) following previous protocols (Dalia et al., 2017; Politan et al., 2025). Acetate and crotonic acid were resolved on a REZEX ROA-Organic Acid H+ (8%) 300 × 7.8 mm column with 3 mM sulfuric acid as the mobile phase at a flow rate of 0.5 mL/min and an oven temperature of 60°C, with detection by DAD at λ = 210 nm; glucose, fructose, sucrose, glycerol, and succinate were detected by refractive index detection at 40°C. The conversion of PHB to crotonic acid was assumed to be 91% based on our recent study (Politan et al., 2025). Raw data were analyzed with chromatographR (Bass, 2023), and peak areas were quantified against standards prepared in ddH_2O.

Kinetic Modelling

We developed a kinetic model to describe PHB production by strain 5X during two-stage, phosphate-limited cultivation on acetate (see Supplementary Methods, Equations 1–9). The model represents the system as four state variables, biomass, acetate, phosphate, and intracellular PHB, whose time evolution is governed by four coupled mass-balance ordinary differential equations (ODEs). Cultivation is treated as two phases, a phosphate-replete growth phase and a phosphate-starvation production phase, separated by a binary switch that activates once phosphate falls below a threshold. Substrate and nutrient kinetics are described by Monod-type rate laws: biomass-specific acetate uptake follows Monod kinetics in acetate with distinct maximal rates in the two phases; phosphate uptake follows Monod kinetics in phosphate and additionally in acetate, so that it ceases when acetate is exhausted; and the biomass-to-acetate yield depends on phosphate, with the specific growth rate given by the product of acetate uptake and yield. PHB productivity is described by a Hill function of both phosphate and acetate. The model comprises 15 parameters; the full equations and parameter definitions are provided in the Supplementary Methods.

The ODEs were solved numerically and the 15 parameters optimized in Python using LMFIT (Newville et al., 2025)

by minimizing the total weighted chi-square (χ^2, the residual between experimental and predicted metabolite concentrations normalized by the experimental standard deviation, summed over the four metabolites and the three initial-phosphate groups; Eq. 10, see Supplementary Methods). The optimized parameters of the ODE model are listed in Table S7. Parameters were bounded between 1.0×10^{-6} and 20.0, except for the Hill coefficients (1.0–5.0) and the biomass yield (0–2.0). Goodness of fit was assessed using the reduced chi-square (χ^2_v, the weighted chi-square divided by the degrees of freedom; Eq. 11). Optimization yielded a total weighted chi-square of 321 and a reduced chi-square of 4.78. Although a reduced chi-square above 1.0 formally indicates underfitting, as the residual variance exceeds the experimental variance, we attribute most of this inflation to the exceptionally small standard deviations of some measurements rather than to a poor description of the data, since the fitted curves reproduced the macroscopic metabolite dynamics across all phosphate regimes (Fig. 3B–E). To prevent the optimization from being biased by data points with disproportionately small variances (often arising

from instrumental error), an error floor of 10% of the mean measured concentration for each triplicate was applied to any standard deviation below this threshold, with a comparable baseline for single-replicate datasets; for PHB data, a fixed baseline error of 0.004 g/L was used in place of the 10% floor under the same rule. All Python optimization scripts and experimental data are available at https://github.com/FritzLabUWA/Vnat-5X-Strain-ODE-kinetic-modelling.git.

Results

Phosphate limitation, not nitrogen, triggers phaBAPC expression and PHB synthesis

To conduct rapid screening of environmental conditions triggering PHB biosynthesis in *V. natriegens*, we built a luminescence-based biosensor for the endogenous *phaBAPC* operon. Aided by *in silico* promoter prediction (LaFleur et al., 2022) (Fig. S1), we defined a 592 bp region upstream of *phaB* as the operon's promoter region, hereafter referred to as the P_{pha} promoter. We then cloned this promoter into a luminescence-based reporter plasmid, transformed it into *V. natriegens* GFN22 (Fig. 1A), and measured the luminescence output of the resulting biosensor strain across phosphate and ammonium concentration gradients. All cultures were grown in MOPS2 minimal medium supplemented with 60.5 mM (5 g/l) sodium acetate as sole carbon source, as reported in a previous study (Politan et al., 2025).

Peak normalized luminescence values across all tested conditions are shown in Fig. 1B and C. We observed that biosensor luminescence output increased above the baseline level only in response to decreasing phosphate concentration. In contrast, nitrogen limitation had no stimulating effect on the activity of the P_{pha} promoter. This finding suggests that the *phaBAPC* operon in *V. natriegens* is regulated by the availability of environmental phosphate, but not nitrogen.

To ascertain whether the observed increase in biosensor luminescence output correlates with PHB accumulation in the parental strain GFN22, we sought to induce expression of the endogenous *phaBAPC* operon via phosphate starvation assays. To this end, cells were washed and resuspended in phosphate-depleted minimal medium once the culture reached exponential phase (OD_{600} ~0.4–0.8) (Fig. 1D). As a negative control, we used a Δ*phaBAPC* mutant of the GFN22 strain, which is deficient in PHB biosynthesis. Cells were stained using BODIPY, a highly specific dye for PHB, to approximate intracellular PHB content via flow cytometry, as reported previously (Kacmar et al., 2006; Politan et al., 2025).

At the onset of the experiment, no noticeable difference in BODIPY fluorescence was observed in both GFN22 and the Δ*phaBAPC* mutant, despite biosensor data suggesting baseline activity of the P_{pha} promoter (Fig. 1E). This could indicate that baseline *phaBAPC* operon expression is insufficient to drive significant flux towards PHB biosynthesis, or limited sensitivity of the BODIPY staining protocol for PHB detection. However, following 24 and 48 hours of phosphate starvation, we observed a 52-fold and 71-fold increase in BODIPY fluorescence, respectively, across the GFN22 population. In comparison, the Δ*phaBAPC* mutant did not show any increase in BODIPY fluorescence, confirming that *V. natriegens* synthesizes PHB under phosphate-limited conditions via expression of the *phaBAPC* operon (Fig. 1E).

This contrasts with previous studies in *Vibrio* species, which have reported PHB accumulation under quorum-sensing-linked or other non-phosphate regulatory regimes (Table S1), rather than in response to phosphate limitation.

Since PHB is an intracellular product, its accumulation may be influenced by cell volume. To provide additional context for the PHB results, forward scatter (FSC) values were examined as an indicative proxy for cell size (Fig. 1E) (McKinnon, 2018). Remarkably, the mean FSC values of the parental strain increased 4.6-fold and 5.7-fold after 24 and 48 hours of phosphate depletion, respectively, indicating cell swelling during PHB accumulation (Fig. 1E). Intriguingly, the Δ*phaBAPC* still displayed a 2.6-fold increase in FSC values, despite the notable absence of PHB production. These observations may reflect broader physiological responses to phosphate starvation, including changes in cell size that are not directly linked to PHB synthesis.

Genome engineering enhances PHB titer and yield

Having established phosphate limitation as a *bona fide* trigger of PHB biosynthesis in *V. natriegens*, we next sought to engineer the strain for higher PHB accumulation. To investigate whether increasing gene dosage of the native *phaBAPC* operon could enhance the rate and extent of PHB biosynthesis, we integrated multiple copies of the operon (each including its native P_{pha} promoter) into *V. natriegens* using the genome engineering toolkit from our recently published Vnat Collection (Faber et al., 2025). This approach aimed to increase PHB biosynthesis without plasmid-based overexpression, antibiotic selection markers, or small molecule inducers, thereby increasing strain stability and reducing operational cost in downstream production settings (Sun et al., 2024). Additionally, target loci for operon integration were strategically selected to eliminate cellular functions that may act as carbon and energy sinks, and thus compete with PHB production. Specifically, the *cps* (capsular exopolysaccharide biosynthesis), *fli* (flagellar biosynthesis), and VNP1 (prophage biosynthesis) loci were targeted to avoid superfluous carbon and energy expenditure. The *phaY* locus, by contrast, was chosen as a dispensable, neutral integration site rather than as a metabolic sink: our previous work showed that deleting the annotated PHA oligomer hydrolases *phaY* and *phaY2* leaves PHB accumulation unchanged (Politan et al., 2025), so replacing *phaY* with an additional operon copy raises gene dosage without removing a function required for production. The resulting mutants were named based on the number of *phaBAPC* operon copies present in their genomes (Fig. 2A). For instance, the strain "3X" harbors a total of three copies of the *phaBAPC* operon, with the two additional copies replacing the *vps* operon (Schulze et al., 2024) and the *phaY* gene, respectively.

The mutants' capacity for PHB production relative to the parental strain GFN22 was examined through phosphate starvation assays as in Fig. 1D. During these experiments, all engineered mutants displayed a ~ 10-fold increase in OD_{600} similar to GFN22 (Fig. 2B), which may be partially attributed to the PHB-dependent cell expansion, the accumulation of biomass, or both, as observed in Fig. 1E. However, both 4X and 5X strains showed significantly higher BODIPY fluorescence compared to GFN22 early in the experiment, indicative of higher baseline *phaBAPC* expression and PHB accumulation (Fig. 2C). After 24

hours, the 4X and 5X strains exhibited ~ 2-fold higher BODIPY values than GFN22, suggesting that enhanced PHB production may result from higher operon copy numbers, deletion of carbon and energy sinks, or a combination thereof.

After 45 h, the final PHB titer was directly quantified via HPLC (Fig. 2D), confirming that strains 4X (0.067 ± 0.010 g/L) and 5X (0.066 ± 0.019 g/L) significantly outperformed the parental strain (0.022 ± 0.020 g/L), while 2X and 3X strains only showed modest, non-significant increases (0.028 ± 0.005 g/L and 0.030 ± 0.008 g/L, respectively). Additionally, while acetate utilization was comparable across strains, the yields were significantly higher in the 3X, 4X, and 5X strains (0.120, 0.134, and 0.130 g/g PHB:acetate, respectively). However, it is yet to be determined whether the observed increases in PHB titer and yield arise from the deletion of specific loci, the overcoming of a gene dosage threshold, or a combined effect of both interventions. The lack of any significant difference between the 4X and 5X strains suggests that further operon integrations do not necessarily lead to additional increases in PHB titer, highlighting a need for further metabolic optimization.

A complementary route to efficient and robust PHB production would be to abolish the host's ability to degrade the polymer, thereby eliminating the risk of polymer mobilization as a result of fluctuating carbon availability. Although deleting the annotated oligomer hydrolases *phaY* and *phaY2* does not prevent PHB turnover (Politan et al., 2025), we reasoned that an unannotated depolymerase might be responsible, as no canonical intracellular PHA depolymerase (PhaZ; EC 3.1.1.75 and 3.1.1.76) has been identified in *V. natriegens* or related *Vibrio* species (De Vogel et al., 2021). We therefore searched the *V. natriegens* genome with profile hidden Markov models of PHA depolymerase families (see Methods) and generated individual deletion mutants at seven candidate loci (Table S2). In a tandem starvation assay (phosphate starvation followed by carbon starvation; Fig. S2), all mutants accumulated PHB normally during phosphate starvation but, like the parental strain, still degraded it upon carbon starvation. This effort was therefore unsuccessful: PHB mobilization in *V. natriegens* appears to proceed through a yet-undiscovered mechanism that, on bioinformatic grounds (De Vogel et al., 2021), may be shared among related *Vibrio* species.

Kinetic modelling predicts the optimal phosphate level for an autonomous two-stage bioprocess

Having characterized phosphate depletion as an environmental trigger of PHB production in *V. natriegens* and constructed engineered strains with enhanced product accumulation during phosphate-limited growth on acetate, we next explored how the best-performing 5X strain may be harnessed in a two-stage bioprocess. Specifically, we investigated how growth and PHB production stages are temporally separated by dynamic phosphate depletion (Fig. 3A).

First, we performed a series of shake-flask experiments to empirically determine how the initial phosphate concentration shapes growth and PHB accumulation. Three initial phosphate levels were selected based on our nutrient limitation analysis (Fig. 1B): high (1.1 mM), intermediate (0.1 mM), and low (0.01 mM), and we tracked acetate and phosphate consumption alongside biomass and PHB

accumulation over time (Fig. 3B-E). PHB was induced in both the intermediate- and low-phosphate groups (Fig. 3E), consistent with phosphate being depleted, and *phaBAPC* expression activated, within the experimental timeframe (Fig. 3D). The high-phosphate group produced no PHB, as acetate ran out before phosphate fell low enough to trigger starvation-induced production (Fig. 3C-D). The intermediate-phosphate group showed a distinct multiphasic response: rapid acetate uptake drove high biomass growth during the phosphate-rich growth phase, followed by a sharp deceleration in both uptake and growth once phosphate dropped below a threshold ($Pi_{threshold}$ = 6.54 ± 0.77 μM) at which PHB production is induced (Fig. 3B).

The two-stage behavior of the intermediate-phosphate culture pointed to an expected trade-off between growth and production: high phosphate channels acetate toward biomass and yields little PHB, whereas very low phosphate limits the biomass available to make PHB. This implies an optimal initial phosphate concentration that balances the two and maximizes titer. To locate this optimum, and to predict PHB production at phosphate levels not tested experimentally, we constructed a mathematical model comprising a system of ordinary differential equations (ODEs) describing the kinetics of cell growth and of acetate, phosphate, and intracellular PHB (see Methods). Growth parameters were optimized by fitting the predicted curves to the experimental data. The fitted model reproduced the macroscopic dynamics of all four state variables across the three phosphate regimes (Fig. 3B-E), confirming that it provides a sound basis for the predictions that follow.

Using the fitted model, we simulated the PHB-to-acetate yield and the final PHB titer across a continuous range of initial phosphate concentrations (Fig. 3G, H). Yield declined monotonically with increasing initial phosphate, confirming the trade-off inferred from the profiling data, and both titer and yield plateaued below the phosphate threshold, consistent with premature starvation that constrains biomass (Fig. 3F) while stabilizing acetate uptake and PHB synthesis. The model identified an optimal initial phosphate concentration of 0.0191 mM, lying between our low- and intermediate-phosphate regimes, with a predicted maximal titer of 0.179 g/L, exceeding the best experimental value under low-phosphate conditions (0.108 ± 0.016 g/L). Experimental validation near this optimum phosphate level (0.021 ± 0.001 mM) yielded a titer of 0.123 ± 0.010 g/L (Table 1), modestly above the low-phosphate condition and suggesting the existence of a well-defined phosphate optimum. At this setting the culture reached a PHB/CDW of 60.5% and a yield of 0.105 ± 0.036 g/g; both remained below the low-phosphate values (69.1% and 0.192 ± 0.041 g/g; Table 1), reflecting the same trade-off, since the optimum maximizes volumetric titer rather than per-cell content or carbon yield. Together, these results demonstrate the predictive utility of the model for tuning phosphate availability to maximize PHB production.

Table 1
PHB production metrics from shake-flasks with varying initial phosphate concentration.

Phosphate Levels	Low	Optimal	Intermediate	High
Final PHB titer (g/L)	0.108 ± 0.016	0.123 ± 0.010	0.068 ± 0.036	0.001 ± 0.000001
CDW (g/L)	0.158 ± 0.013	0.220 ± 0.064	0.499 ± 0.109	0.701 ± 0.023
PHB (%CDW)	69.1 ± 12.0	60.5 ± 18.7	13.0 ± 4.0	0.156 ± 0.005
g PHB produced/ g Acetate (%)	19.2 ± 4.1	10.5 ± 3.6	1.66 ± 0.90	0.032 ± 0.003

Note. Standard deviation (SD) presented in this table are SD before 10% error floor is applied.

Phosphate limitation drives PHB synthesis across diverse carbon sources

We next asked whether the phosphate-starvation strategy extends to carbon sources other than acetate. We had previously found *phaBAPC* expression to be partially carbon-source dependent (Politan et al., 2025), so the operon responds to more than one input and the strength of the phosphate response could vary from substrate to substrate. We therefore tested strain 5X on five further substrates, each carbon-equivalent to the 60.5 mM sodium acetate used above: 40.3 mM glycerol, 30.3 mM disodium succinate, 20.2 mM glucose, 20.2 mM fructose, and 10.1 mM sucrose (Fig. 4). Media containing non-sodium carbon sources were supplemented with 60.5 mM NaCl, so that sodium was constant across all six conditions.

Washing into phosphate-free medium, the regime used for the copy-number comparison (Fig. 2), removes external phosphate entirely, and phosphate is also required to regenerate ATP, so complete removal limits the metabolism that has to continue if polymer is to accumulate. For the substrate comparison we therefore induced by diluting pelleted mid-exponential precultures (OD_{600} 0.4–0.5) 1:200 into phosphate-free medium, which leaves a residual phosphate carry-over of approximately 2.5 µM, about 1:200 of the ~ 0.5 mM estimated to be present in the preculture, and keeps cells metabolically active while still triggering *phaBAPC* induction. All six conditions were induced in this way. On acetate, the dilution-based protocol increased acetate consumption (Fig. 4B) and raised the final PHB titer of strain 5X to 0.18 ± 0.12 g/L (Fig. 4C), against 0.066 ± 0.019 g/L after washing into phosphate-free medium (Fig. 2D) and 0.123 ± 0.010 g/L under autonomous phosphate exhaustion (Fig. 3E).

Among the substrates tested, after 48 h of phosphate starvation fructose supported the highest intracellular PHB accumulation (quantified by mean BODIPY signal, Fig. 4A), closely followed by glucose. In contrast, succinate-fed cultures exhibited the lowest fluorescence signal. Notably, glucose- and sucrose-fed cultures displayed pronounced inter-replicate variability, with up to fivefold differences in BODIPY signal between biological replicates (Fig. 4A), a phenomenon not observed for the other carbon sources tested. To contextualize these differences, we quantified substrate consumption during

fermentation. Acetate and glycerol were only partially consumed after 48 h (53% and 62%, respectively; Fig. 4B). In contrast, succinate, fructose, and sucrose were fully depleted within 48 hours.

For glucose, the variable PHB accumulation between biological replicates correlated with substrate consumption, where low PHB levels coincide with low glucose consumption (i.e. high residual extracellular glucose) and *vice versa*, suggesting highly variable glucose metabolism in our phosphate-starvation setup with potential regulatory effects on the *pha* operon. Comparison of final titer and yield at 48 h revealed clear substrate-dependent differences in process performance (Fig. 4C–D). Fructose supported the highest PHB titer (0.74 ± 0.17 g/L; yield 0.21 ± 0.05 g/g), significantly exceeding acetate by roughly fourfold in titer and more than twofold in yield (acetate yield 0.09 ± 0.03 g/g). The second highest titer was achieved with glucose (0.55 ± 0.34 g/L), with a significantly higher yield than acetate (0.21 ± 0.04 g/g). Glycerol achieved a titer of 0.46 ± 0.27 g/L with the highest observed yield (0.22 ± 0.12 g/g). Succinate performed the poorest, with a titer comparable to acetate and the lowest yield (0.053 ± 0.015 g/g).

Together, these findings show that phosphate starvation activates the *phaBAPC* operon regardless of the carbon source and indicate that sugar-based substrates and glycerol outperform acetate as feedstocks for phosphate starvation-driven PHB production.

Discussion

In this study we established that the marine bacterium *V. natriegens* accumulates PHB under phosphate limitation, and we exploited this native response to build an autonomous, inducer-free two-stage process for PHB production from acetate. Using a transcriptional biosensor of the *phaBAPC* operon we identified phosphate, rather than nitrogen, as the signal that triggers polymer synthesis; we then raised PHB titer by integrating additional chromosomal copies of the operon and used a kinetic model to define a nutrient regime that maximizes production. Because the switch from growth to production is operated by the cells' own consumption of phosphate, the process requires no chemical inducer, no engineered regulatory circuit, and no active nutrient feeding or two-vessel system to initiate accumulation.

Regulation of PHB synthesis by phosphate

In other *Vibrio* species, PHB accumulation has been linked to carbon source, nitrogen availability, salinity, oxygenation, or quorum sensing, but not, to our knowledge, to phosphate limitation (Table S1; (Boyandin et al., 2008; Hong et al., 2019; Li et al., 2021; Miyamoto et al., 1998; Mohandas et al., 2017; Sasidharan et al., 2015; Schwartzman et al., 2022; Wei et al., 2011; Yévenes et al., 2021)

). Quorum-sensing control has been demonstrated in *Vibrio harveyi* (Miyamoto et al., 1998; Sun et al., 1994) and, more recently, in *Vibrio scophthalmi*, where a *luxR* deletion lowers transcription of the PHA biosynthetic genes and intracellular PHA content (Seok et al., 2024). Outside the genus, the closest case is the marine alphaproteobacterium *Pseudovibrio* sp. FO-BEG1, in which phosphate limitation triggers PHA accumulation and a pho box lies upstream of a phasin gene (Romano et al., 2015). The functional

evidence comes from *Acinetobacter*, where a second promoter upstream of *phaB* is induced twenty-fold by phosphate starvation and that induction is lost in an *E. coli phoB* background (Schembri et al., 1995). That promoter also carries a pho box, the 18 bp motif bound by phosphorylated PhoB. Together with the loss of induction in the *phoB* background, this places the *Acinetobacter* PHA genes within the Pho regulon, the phosphate-starvation response controlled by the two-component system PhoB-PhoR (Hsieh and Wanner, 2010; Torriani, 1990). The induction of the native P_{pha} promoter we observe is consistent with analogous Pho-dependent control in *V. natriegens*, which will be described in more detail in a separate publication (in preparation).

The *pha* biosensor also responded to the carbon source, with a raised baseline on acetate and pronounced variability on glucose (Figs. 1, 4). This may indicate carbon-catabolite (CRP-dependent) regulation, consistent with our earlier finding that the *pha* operon is upregulated during growth on acetate compared to glucose (Politan et al., 2025). Phosphate starvation nonetheless drove PHB accumulation on all six carbon sources tested (Fig. 4), each of which is catabolized to acetyl-CoA. At the enzymatic level, flux into PHB is set largely by the size of that acetyl-CoA pool. In recombinant *E. coli*, PHB flux responds to the acetyl-CoA/CoA ratio with a coefficient of 0.8, against 0.25 for the $NADPH/NADP^+$ ratio (van Wegen et al., 2001). Phosphate limitation arrests growth while acetate uptake continues, so acetyl-CoA accumulates and free CoA falls. Together with induction of the *pha* operon (Fig. 1B, C), this accounts for PHB accumulating as growth stops (Fig. 3B, E). In future work, measuring acetyl-CoA, adenylate and pyridine nucleotide pools across the switch would separate the transcriptional and metabolic contributions.

Phosphate depletion as an autonomous two-stage switch

The trade-off between biomass formation and product synthesis is usually resolved with an engineered switch, whether a chemical inducer, a quorum-sensing circuit or a stationary-phase promoter (Dinh and Prather, 2019; Gupta et al., 2017; Tan and Prather, 2017; Venayak et al., 2018), each of which has been applied to PHB production (He et al., 2017). The alternative is to let the culture set the switch by consuming a medium component, and phosphate has a long record in that role. The highest PHB titer reported, 232 g/L at 80% of cell dry weight, came from a 60 L fed-batch of *Cupriavidus necator* in which accumulation was induced by phosphate limitation in place of nitrogen limitation (Ryu et al., 1997). That choice also frees ammonia for pH control. Phosphorus limitation likewise outperformed nitrogen limitation in *Burkholderia sacchari* (Oliveira-Filho et al., 2020). Beyond PHA, phosphate depletion is now used as a scale-invariant autoinduction signal. A PhoB-dependent promoter in *E. coli* yields up to 8.1 g/L recombinant protein with no inducer, and performs consistently from 20 µL microtiter wells to 1 L bioreactors (Menacho-Melgar et al., 2020). The same trigger has been used for two-stage dynamic metabolic control at 4,000 L (Ye et al., 2021). Native, unmodified pho promoters serve this purpose in *E. coli* and *Pseudomonas putida*, where the cell density at which the promoter is activated scales linearly with the initial phosphate concentration (Torres-Bacete et al., 2021).

What has not been shown before is that the native, unmodified promoter of a PHB biosynthetic operon responds to phosphate directly in a *Vibrio*, so that polymer accumulation is timed by the cells' own phosphate consumption with no synthetic regulatory layer. The switch point is then set by a single medium parameter at inoculation, which makes the kinetic model a design tool (Fig. 3F-H). Inducer-free operation also lowers cost, since IPTG at a bulk price of US$356/kg accounted for 9.8 to 28.2% of variable operating cost in a recent industrial fermentation analysis (Cunniffe et al., 2025; Shariati et al., 2021). Because the response is transcriptional, any gene placed under P_{pha} would be switched on when phosphate runs out. The same trigger can therefore be used for two-stage production of products other than PHB in *V. natriegens*.

Optimizing phosphate-controlled PHB production

Operon engineering and model-guided process optimization raised the PHB titer from 0.022 g/L in the parental strain (wash-based starvation, Fig. 2D) to 0.123 g/L in the 5X strain (autonomous phosphate exhaustion, Table 1), with up to 69.1% PHB per cell dry weight. For an inducer-free shake-flask process on acetate that polymer content is high, and it was reached without the complex nitrogen supplementation that raises PHB titer sixtyfold in a plasmid-based *E. coli* system (Chen et al., 2018). It exceeds our previous plasmid-based result in *V. natriegens* (45.7%; (Politan et al., 2025)) and the highest value reported for an engineered *Vibrio* sp. dhg (65.7%, in fed-batch (Kim et al., 2026)). The titer is of the same order as the shake-flask benchmarks on acetate, 0.11 g/L for engineered *Halomonas* sp. JJY01 (Park et al., 2024) and 0.46 g/L at 38% PHB/CDW for *C. necator* on acetogen-derived acetate (Ren and Ninomiya, 2025).

A higher titer requires more biomass at the point where phosphate runs out, and in a two-stage fermentation the phosphate feed sets that point directly. Cells are grown to the intended density while phosphate is supplied, and production begins when the feed is stopped. Phosphate can also be held just below $Pi_{threshold}$ by intermittent low-level feeding, which our model predicts and which is simple to implement in a controlled bioreactor (Fig. 3F-H). The second regime may be preferable, because acetate activation consumes ATP through either acetate kinase or AMP-forming acetyl-CoA synthetase (Wolfe, 2005), and ATP regeneration requires orthophosphate, so acetyl-CoA supply should fall if phosphate is withdrawn completely (Schuhmacher et al., 2014). High-cell-density fed-batch routinely takes acetate-fed strains into the tens of g/L (Tao et al., 2022), so the required biomass is attainable.

Phosphate starvation also enlarged the cells, raising mean forward scatter 4.6-fold at 24 h and 5.7-fold at 48 h (Fig. 1E). The Δ*phaBAPC* mutant enlarged 2.6-fold without making any polymer, so the increase is part of the starvation response and does not only depend on granule formation. Phosphate limitation is coupled to elongation and PHA accumulation in the same way in *Pseudovibrio* sp. FO-BEG1 (Romano et al., 2015). Because PHB is stored intracellularly, larger cells hold more of it, and PHB content more than doubled in *E. coli* when cell division was inhibited or the cytoskeleton weakened (Jiang et al., 2015; Wu et al., 2016). A morphology-engineered *Halomonas bluephagenesis* reached 149 g/L cell dry weight at 82% PHB in a 5,000 L bioreactor (Chen et al., 2025). *V. natriegens* enlarges under the same condition that

induces the operon, so cell size and polymer synthesis are already coupled without a division-inhibition circuit. Whether that native increase is sufficient, or whether the larger cells obtained by inhibiting division in *E. coli* and *H. bluephagenesis* would add further polymer, could be tested by placing a division inhibitor under phosphate control, so that enlargement and induction follow from the same signal.

A marine origin for phosphate control of PHB

Why phosphate rather than nitrogen should be the trigger in this organism is unresolved, but its habitat suggests an explanation. Phosphorus is scarce enough to limit microbial processes in a range of marine systems, including the eastern Mediterranean and the subtropical North Atlantic (Thingstad et al., 2005; Wu et al., 2000). The phosphorus regime of an ocean basin is also reflected in the gene content of its resident bacteria. Comparing Atlantic and Pacific populations of the same species, almost all of the genes differing significantly in abundance are phosphorus-acquisition genes, enriched in the phosphorus-poor Atlantic (Coleman and Chisholm, 2010). *V. natriegens* was isolated from salt marsh mud from a barrier island in the coastal Atlantic (Wang et al., 2013). In a pristine salt marsh in South Carolina, phosphorus limited the soil bacterial community while nitrogen limited the plants (Sundareshwar et al., 2003). In such estuarine water, phosphate turnover times fall to 3 to 10 minutes during the spring bloom, when phosphorus is the limiting nutrient (Fisher et al., 1992). A fast-growing copiotroph consuming a pulse of carbon grows until the nutrient in shortest supply relative to its biomass requirement is exhausted, and carbon taken up beyond that point cannot be used for growth. Storage polymers accommodate the excess and thereby decouple carbon uptake from biomass formation (Mason-Jones et al., 2022). If phosphate is the nutrient that runs out first in this habitat, then phosphate control of the *pha* operon would start polymer synthesis at the point where carbon begins to accumulate in excess. In *V. cholerae* the Pho regulon extends beyond phosphate scavenging to motility, biofilm formation and c-di-GMP metabolism (Pratt et al., 2010, 2009), so a phosphate signal is already used in *Vibrio* to reorganize cell behavior.

In summary, *V. natriegens* naturally produces PHB under phosphate limitation, and we have demonstrated how this response can be harnessed to establish an autonomous, inducer-free two-stage biosynthetic process whose performance we improved by strain engineering and rationalized with a predictive kinetic model. Although production titer, rate, and yield are not yet competitive, the combination of a self-actuating trigger, a fast-growing and salt-tolerant host, feedstock flexibility, and defined engineering levers (e.g. continuous sub-threshold phosphate feeding and morphology engineering) makes *V. natriegens* a compelling platform for sustainable production of PHB and other bioproducts.

Declarations

Competing interests

Woodside Energy Ltd co-funded the Australian Research Council Linkage Project under which this work was carried out. The two colleagues thanked in the Acknowledgements for input and discussions, Dr

Jitendra Joshi and Dr Sahil Garg, were affiliated with Woodside Energy Ltd during this work, and Dr Joshi has since left the company. Woodside reviewed the manuscript before submission, and the authors retained full control over its content and over the decision to submit. No author is employed by, or holds a financial interest in, Woodside Energy Ltd. The authors have no other financial or non-financial interests to disclose.

Declaration of generative AI and AI-assisted technologies in the writing process

During the preparation of this work, the authors used ChatGPT to improve the readability and language clarity of the manuscript. After using this tool, the authors reviewed and edited the content as needed and took full responsibility for the content of the published article.

Author contributions

R.J.P. conceptualized the study, developed the strains, performed the experiments unless otherwise indicated, analyzed the data, and wrote, reviewed and edited the manuscript, including the figures. J.Z.W. performed experiments and developed the modelling analysis, including the modelling section and its associated figures and table (Fig. 3, Fig. S3 and Table S7). K.M.M. developed the plasmids and strains, and performed the experiments presented in Fig. 1A–C with S.D.V. B.F.B. assisted with data acquisition and HPLC analysis, and reviewed and edited the manuscript. B.R.K.R. provided methodology for flow cytometry and HPLC, confirmed phosphate-dependent PHB production, and contributed to the interpretation and discussion of the results. G.R.F. provided HPLC instrumentation and expertise, and assisted with method development. S.D.V. provided guidance on in silico promoter prediction (Fig. S1) and depolymerase candidate identification (Fig. S2), supervised J.Z.W. in the modelling analysis (Fig. S3 and Table S7), and reviewed and edited the manuscript. G.F. conceptualized and supervised the project, contributed to the interpretation and discussion of the results, and reviewed and edited the manuscript. All authors reviewed and approved the final manuscript.

Ethical Approval

Not applicable. This study did not involve human participants, human data or animals.

Funding

This work was funded by the Australian Research Council and Woodside Energy Ltd through Linkage Project LP220100185, and by the Australian Research Council through Future Fellowship FT230100283 to G. Fritz. The views expressed are those of the authors and do not necessarily reflect the views of the funding partners.

Availability of data and materials

The kinetic model code and the experimental data used for parameter fitting are available in the FritzLabUWA/Vnat-5X-Strain-ODE-kinetic-modelling repository on GitHub, at

https://github.com/FritzLabUWA/Vnat-5X-Strain-ODE-kinetic-modelling. The remaining datasets generated and analyzed during this study, including the plate reader, flow cytometry and HPLC measurements underlying Figs. 1, 2 and 4 and the supplementary figures, are available from the corresponding authors on reasonable request. The strains and plasmids generated in this study are available from the corresponding authors on request.

References

1. Anderson AJ, Dawes EA (1990) Occurrence, metabolism, metabolic role, and industrial uses of bacterial polyhydroxyalkanoates. Microbiol Rev 54:450–472. https://doi.org/10.1128/mr.54.4.450-472.1990
2. Babel W, Steinbüchel A (2003) Biopolyesters, Technology & Engineering. Springer
3. Bass E (2023) chromatographR: Chromatographic data analysis toolset (version 0.7.1). https://doi.org/http://doi.org/10.5281/zenodo.6944334
4. Boyandin A, Kalacheva GS, Medvedeva S, Rodicheva E, Volova TG (2008) Luminous Bacteria as Producers of Polyhydroxyalkanoates. Macromol. Symp. 269, 17–22. https://doi.org/10.1002/masy.200850904
5. Chen G, Li J, Sun Y, Wang Z, Leeke GA, Moretti C, Cheng Z, Wang Y, Li N, Mu L, Li, Jinyu, Tao J, Yan B, Hou L (2024) Replacing Traditional Plastics with Biodegradable Plastics. Impact Carbon Emissions Eng 32:152–162. https://doi.org/10.1016/j.eng.2023.10.002
6. Chen J, Li W, Zhang Z-Z, Tan T-W, Li Z-J (2018) Metabolic engineering of *Escherichia coli* for the synthesis of polyhydroxyalkanoates using acetate as a main carbon source. Microb Cell Factories 17:102. https://doi.org/10.1186/s12934-018-0949-0
7. Chen Y-L, Liu X, Zhang L-Z, Yang J-S, Guo W-K, Zheng S, Wang J-L, Wu F-Q, Yan X, Wu Q, Chen G-Q (2025) Cell Sizes Matter for Industrial Bioproduction, a Case of Polyhydroxybutyrate. Adv Sci 12:2412256. https://doi.org/10.1002/advs.202412256
8. Choi J, Lee SY (1999) Factors affecting the economics of polyhydroxyalkanoate production by bacterial fermentation. Appl Microbiol Biotechnol 51:13–21. https://doi.org/10.1007/s002530051357
9. Coleman ML, Chisholm SW (2010) Ecosystem-specific selection pressures revealed through comparative population genomics. Proc. Natl. Acad. Sci. 107, 18634–18639. https://doi.org/10.1073/pnas.1009480107
10. Cunniffe J, Berrio VR, Hunter C, Nguyen T, Salmon S, Crook N, Grunden A, Sagues WJ (2025) Techno-economic analysis of industrial-scale fermentation for formate dehydrogenase (FDH) production. Bioresour Bioprocess 12:145. https://doi.org/10.1186/s40643-025-00985-3
11. Dalia TN, Hayes CA, Stolyar S, Marx CJ, Mckinlay JB, Dalia AB (2017) Multiplex genome editing by natural transformation (MuGENT) for synthetic biology in *Vibrio natriegens*. ACS Synth Biol 6:1650–1655. https://doi.org/10.1021/acssynbio.7b00116

12. De Vogel FA, Schlundt C, Stote RE, Ratto JA, Amaral-Zettler LA (2021) Comparative Genomics of Marine Bacteria from a Historically Defined Plastic Biodegradation Consortium with the Capacity to Biodegrade Polyhydroxyalkanoates. Microorganisms 9:186. https://doi.org/10.3390/microorganisms9010186
13. Della Valle S, Faber A, Politan RJ, Lama S, Fritz G (2025) From marsh to market: taming *Vibrio natriegens* for sustainable bioproduction. Curr Opin Biotechnol 96:103353. https://doi.org/10.1016/j.copbio.2025.103353
14. Dinh CV, Prather KLJ (2019) Development of an autonomous and bifunctional quorum-sensing circuit for metabolic flux control in engineered *Escherichia coli.* Proc. Natl. Acad. Sci. 116, 25562–25568. https://doi.org/10.1073/pnas.1911144116
15. Eagon RG (1961) Pseudomonas natriegens, a marine bacterium with a generation time of less than 10 minutes 301, 1961–1962
16. Faber A, Politan R, Nicol A, Valle SD, Jenkins B, Fritz G, n.d. Mitigating protocatechuic acid toxicity in *Vibrio natriegens* enables poly-3-hydroxybutyrate production from an aromatic carbon source
17. Faber A, Politan RJ, Stukenberg D, Morris K, Kim R, Jeon E, Inckemann R, Becker A, Thuronyi B, Fritz G (2025) Expanding genetic engineering capabilities in *Vibrio natriegens* with the Vnat Collection. https://doi.org/https://doi.org/10.1093/nar/gkaf580. Nucleic Acids Res
18. Fisher TR, Peele ER, Ammerman JW, Harding LW (1992) Nutrient limitation of phytoplankton in Chesapeake Bay. Mar Ecol Prog Ser 82:51–63
19. Geyer R, Jambeck JR, Law KL (2017) Production, use, and fate of all plastics ever made. Sci Adv 3:e1700782. https://doi.org/10.1126/sciadv.1700782
20. Groher A, Weuster-Botz D (2016) Comparative reaction engineering analysis of different acetogenic bacteria for gas fermentation. J Biotechnol 228:82–94. https://doi.org/10.1016/j.jbiotec.2016.04.032
21. Gupta A, Reizman IMB, Reisch CR, Prather KLJ (2017) Dynamic regulation of metabolic flux in engineered bacteria using a pathway-independent quorum-sensing circuit. Nat Biotechnol 35:273–279. https://doi.org/10.1038/nbt.3796
22. Hädrich M, Schulze C, Hoff J, Blombach B (2024) *Vibrio natriegens*: Application of a Fast. https://doi.org/10.1007/10_2024_271. -Growing Halophilic Bacterium
23. He X, Chen Y, Liang Q, Qi Q (2017) Autoinduced AND Gate Controls Metabolic Pathway Dynamically in Response to Microbial Communities and Cell Physiological State. ACS Synth Biol 6:463–470. https://doi.org/10.1021/acssynbio.6b00177
24. Hoff J, Daniel B, Stukenberg D, Thuronyi BW, Waldminghaus T, Fritz G (2020) *Vibrio natriegens*: an ultrafast-growing marinebacterium as emerging synthetic biology chassis. Environ Microbiol. https://doi.org/doi:10.1111/1462-2920.15128
25. Hong J-W, Song H-S, Moon Y-M, Hong Y-G, Bhatia SK, Jung H-R, Choi T-R, Yang S, Park H-Y, Choi Y-K, Yang Y-H (2019) Polyhydroxybutyrate production in halophilic marine bacteria *Vibrio proteolyticus*

isolated from the Korean peninsula. Bioprocess Biosyst Eng 42:603–610. https://doi.org/10.1007/s00449-018-02066-6

26. Hsieh Y-J, Wanner BL (2010) Global regulation by the seven-component Pi signaling system. Curr Opin Microbiol Cell Regul 13:198–203. https://doi.org/10.1016/j.mib.2010.01.014
27. Jiang X-R, Wang H, Shen R, Chen G-Q (2015) Engineering the bacterial shapes for enhanced inclusion bodies accumulation. Metab Eng 29:227–237. https://doi.org/10.1016/j.ymben.2015.03.017
28. Jin J, Wicks J, Min Q, Li J, Hu Y, Ma J, Wang Y, Jiang Z, Xu Y, Lu R, Si G, Papangelakis P, Shakouri M, Xiao Q, Ou P, Wang X, Chen Z, Zhang W, Yu K, Song J, Jiang X, Qiu P, Lou Y, Wu D, Mao Y, Ozden A, Wang C, Xia BY, Hu X, Dravid VP, Yiu Y-M, Sham T-K, Wang Z, Sinton D, Mai L, Sargent EH, Pang Y (2023) Constrained C2 adsorbate orientation enables CO-to-acetate electroreduction. Nature 617:724–729. https://doi.org/10.1038/s41586-023-05918-8
29. Kacmar J, Carlson R, Balogh SJ, Srienc F (2006) Staining and quantification of poly-3-hydroxybutyrate in *Saccharomyces cerevisiae* and *Cupriavidus necator* cell populations using automated flow cytometry. Cytometry 69:27–35. https://doi.org/10.1002/cyto.a.20197
30. Kadouri D, Jurkevitch E, Okon Y, Castro-Sowinski S (2005) Ecological and Agricultural Significance of Bacterial Polyhydroxyalkanoates. Crit Rev Microbiol 31:55–67. https://doi.org/10.1080/10408410590899228
31. Kanehisa M (2002) The KEGG databases at GenomeNet. Nucleic Acids Res 30:42–46. https://doi.org/10.1093/nar/30.1.42
32. Kim K, Kim DN, Kang C, Kang YJ, Lee HK, Noh MH, Jung GY, Seo SW (2026) Direct conversion of brown macroalgae into polyhydroxybutyrate using engineered *Vibrio* sp. dhg. Chem Eng J 532:174264. https://doi.org/10.1016/j.cej.2026.174264
33. Knoll M, Hamm TM, Wagner F, Martinez V, Pleiss J (2009) The PHA Depolymerase Engineering Database: A systematic analysis tool for the diverse family of polyhydroxyalkanoate (PHA) depolymerases. BMC Bioinformatics 10:89. https://doi.org/10.1186/1471-2105-10-89
34. Koller M, Braunegg G (2018) Advanced approaches to produce polyhydroxyalkanoate (PHA) biopolyesters in a sustainable and economic fashion. EuroBiotech J 2:89–103. https://doi.org/10.2478/ebtj-2018-0013
35. LaFleur TL, Hossain A, Salis HM (2022) Automated model-predictive design of synthetic promoters to control transcriptional profiles in bacteria. Nat Commun 13:5159. https://doi.org/10.1038/s41467-022-32829-5
36. Li H-F, Wang M-R, Tian L-Y, Li Z-J (2021) Production of Polyhydroxyalkanoates (PHAs) by *Vibrio alginolyticus* Strains Isolated from Salt Fields. Molecules 26:6283. https://doi.org/10.3390/molecules26206283
37. Li H-H, Wu, Jie, Liu J-Q, Wu Q-Z, He R, Cheng Z-H, Lv J-L, Lin W-Q, Wu J, Liu D-F, Li W-W (2023) Nonsterilized fermentation of crude glycerol for polyhydroxybutyrate production by metabolically

engineered *Vibrio natriegens*. ACS Synth Biol 12:3454–3462. https://doi.org/10.1021/acssynbio.3c00498

38. Mason-Jones K, Robinson SL, Veen GF, Ciska), Manzoni S, van der Putten WH (2022) Microbial storage and its implications for soil ecology. ISME J 16:617–629. https://doi.org/10.1038/s41396-021-01110-w
39. McKinnon KM (2018) Flow Cytometry: An Overview. Curr Protoc Immunol 120. https://doi.org/10.1002/cpim.40
40. Menacho-Melgar R, Ye Z, Moreb EA, Yang T, Efromson JP, Decker JS, Wang R, Lynch MD (2020) Scalable, two-stage, autoinduction of recombinant protein expression in *E. coli* utilizing phosphate depletion. Biotechnol Bioeng 117:2715–2727. https://doi.org/10.1002/bit.27440
41. Miyamoto CM, Sun W, Meighen EA (1998) The LuxR regulator protein controls synthesis of polyhydroxybutyrate in *Vibrio harveyi*. Biochim Biophys Acta 1384:356–364
42. Mohandas SP, Balan L, Lekshmi N, Cubelio SS, Philip R, Singh B, I.S (2017) Production and characterization of polyhydroxybutyrate from *Vibrio harveyi* MCCB 284 utilizing glycerol as carbon source. J Appl Microbiol 122:698–707. https://doi.org/10.1111/jam.13359
43. Moreira JPC, Heap JT, Alves JI, Domingues L (2023) Developing a genetic engineering method for *Acetobacterium wieringae* to expand one-carbon valorization pathways. Biotechnol Biofuels Bioprod 16:24. https://doi.org/10.1186/s13068-023-02259-6
44. Newville M, Stensitzki T, Allen DB, Ingargiola A (2025) LMFIT: Non-Linear Least-Square Minimization and Curve-Fitting for Python (1.3.4). Zenodo
45. Oliveira-Filho ER, Silva JGP, De Macedo MA, Taciro MK, Gomez JGC, Silva LF (2020) Investigating Nutrient Limitation Role on Improvement of Growth and Poly(3-Hydroxybutyrate) Accumulation by *Burkholderia sacchari* LMG 19450 From Xylose as the Sole Carbon Source. Front Bioeng Biotechnol 7:416. https://doi.org/10.3389/fbioe.2019.00416
46. Park J-K, Jeon J-M, Yang Y-H, Kim S-H, Yoon J-J (2024) Efficient polyhydroxybutyrate production using acetate by engineered *Halomonas* sp. JJY01 harboring acetyl-CoA acetyltransferase. Int J Biol Macromol 254:127475. https://doi.org/10.1016/j.ijbiomac.2023.127475
47. Plastics – the fast Facts 2024 • Plastics Europe, 2004. Plast. Eur. URL https://plasticseurope.org/knowledge-hub/plastics-the-fast-facts-2024/ (accessed 6.3.26)
48. Pohlmann A, Fricke WF, Reinecke F, Kusian B, Liesegang H, Cramm R, Eitinger T, Ewering C, Pötter M, Schwartz E, Strittmatter A, Voß I, Gottschalk G, Steinbüchel A, Friedrich B, Bowien B (2006) Genome sequence of the bioplastic-producing Knallgas bacterium *Ralstonia eutropha* H16. Nat Biotechnol 24:1257–1262. https://doi.org/10.1038/nbt1244
49. Politan RJ, Della Valle S, Pineda L, Joshi J, Euler C, Flematti G, Fritz G (2025) Establishing *Vibrio natriegens* as a high-performance host for acetate-based poly-3-hydroxybutyrate production. Metab Eng 92:22–38. https://doi.org/10.1016/j.ymben.2025.07.003
50. Pratt JT, Ismail AM, Camilli A (2010) PhoB regulates both environmental and virulence gene expression in *Vibrio cholerae*. Mol Microbiol 77:1595–1605. https://doi.org/10.1111/j.1365-

2958.2010.07310.x

51. Pratt JT, McDonough E, Camilli A (2009) PhoB Regulates Motility, Biofilms, and Cyclic di-GMP in *Vibrio cholerae*. J Bacteriol 191:6632–6642. https://doi.org/10.1128/jb.00708-09
52. Ren H, Ninomiya K (2025) Acetate-mediated two-stage microbial production of poly[(*R*)-3-hydroxybutyrate] (PHB) from CO2 and H2 using a synthetic medium free of vitamins and cysteine. J Biosci Bioeng 140:42–49. https://doi.org/10.1016/j.jbiosc.2025.04.004
53. Riedel SL, Bader J, Brigham CJ, Budde CF, Yusof ZAM, Rha C, Sinskey AJ (2012) Production of poly(3-hydroxybutyrate-co-3-hydroxyhexanoate) by *Ralstonia eutropha* in high cell density palm oil fermentations. Biotechnol Bioeng 109:74–83. https://doi.org/10.1002/bit.23283
54. Romano S, Schulz-Vogt HN, González JM, Bondarev V (2015) Phosphate Limitation Induces Drastic Physiological Changes, Virulence-Related Gene Expression, and Secondary Metabolite Production in *Pseudovibrio* sp. Strain FO-BEG1. Appl Environ Microbiol 81:3518–3528. https://doi.org/10.1128/AEM.04167-14
55. Rosenboom J-G, Langer R, Traverso G (2022) Bioplastics for a circular economy. Nat Rev Mater 7:117–137. https://doi.org/10.1038/s41578-021-00407-8
56. Ryu HW, Hahn SK, Chang YK, Chang HN (1997) Production of Poly(3-hydroxybutyrate) by High Cell Density Fed-Batch Culture of *Alcaligenes eutrophus* with Phosphate Limitation. Biotechnol. Bioeng. 55, 28–32. https://doi.org/doi:%2010.1002/(SICI)1097-0290(19970705)55:1%3C28::AID-BIT4%3E3.0.CO;2-Z
57. Sasidharan RS, Bhat SG, Chandrasekaran M (2015) Biocompatible polyhydroxybutyrate (PHB) production by marine *Vibrio azureus* BTKB33 under submerged fermentation. Ann Microbiol 65:455–465. https://doi.org/10.1007/s13213-014-0878-z
58. Schembri MA, Bayly RC, Davies JK (1995) Phosphate concentration regulates transcription of the *Acinetobacter* polyhydroxyalkanoic acid biosynthetic genes. J Bacteriol 177:4501–4507. https://doi.org/10.1128/jb.177.15.4501-4507.1995
59. Schuhmacher T, Löffler M, Hurler T, Takors R (2014) Phosphate limited fed-batch processes: Impact on carbon usage and energy metabolism in *Escherichia coli*. J Biotechnol Genomics Revolution its Impact Future Biotechnol 190:96–104. https://doi.org/10.1016/j.jbiotec.2014.04.025
60. Schulze C, Hädrich M, Borger J, Rühmann B, Döring M, Sieber V, Thoma F, Blombach B (2024) Investigation of exopolysaccharide formation and its impact on anaerobic succinate production with *Vibrio natriegens*. Microb Biotechnol 17:e14277. https://doi.org/10.1111/1751-7915.14277
61. Schwartzman JA, Ebrahimi A, Chadwick G, Sato Y, Roller BRK, Orphan VJ, Cordero OX (2022) Bacterial growth in multicellular aggregates leads to the emergence of complex life cycles. Curr Biol 32:3059–3069e7. https://doi.org/10.1016/j.cub.2022.06.011
62. Seok B, Kim MS, Kim BS (2024) Genome-wide analysis of quorum sensing regulon in marine fish pathogen *Vibrio scophthalmi*. Sci Rep 14:27740. https://doi.org/10.1038/s41598-024-78803-7
63. Shariati FS, Keramati M, Valizadeh V, Cohan RA, Norouzian D (2021) Comparison of *E. coli* based self-inducible expression systems containing different human heat shock proteins. Sci Rep 11:4576.

https://doi.org/10.1038/s41598-021-84188-8

64. Stukenberg D, Faber A, Becker A (2024) Graded-CRISPRi, a tool for tuning the strengths of CRISPRi-mediated knockdowns in *Vibrio natriegens* using gRNA libraries. ACS Synth Biol. https://doi.org/10.1021/acssynbio.4c00056. acssynbio.4c00056
65. Stukenberg D, Hensel T, Hoff J, Daniel B, Inckemann R, Tedeschi JN, Nousch F, Fritz G (2021) The Marburg collection: A Golden Gate DNA assembly framework for synthetic biology applications in *Vibrio natriegens*. ACS Synth Biol 10:28. https://doi.org/10.1021/acssynbio.1c00126
66. Stukenberg D, Hoff J, Faber A, Becker A (2022) NT-CRISPR, combining natural transformation and CRISPR-Cas9 counterselection for markerless and scarless genome editing in *Vibrio natriegens*. Commun Biol 5:265. https://doi.org/10.1038/s42003-022-03150-0
67. Sun D, Li H-H, Wu, Jing, Wu J, Lin W-Q, He R-L, Liu D-F, Li W-W (2024) Antibiotics-Free Steady Bioproduction of Valuable Chemicals from Organic Wastes by Engineered *Vibrio natriegens* through Targeted Gene Integration. ACS Synth Biol 13:4233–4244. https://doi.org/10.1021/acssynbio.4c00669
68. Sun W, Cao JG, Teng K, Meighen EA (1994) Biosynthesis of poly-3-hydroxybutyrate in the luminescent bacterium, *Vibrio harveyi*, and regulation by the lux autoinducer, N-(3-hydroxybutanoyl)homoserine lactone. J Biol Chem 269:20785–20790. https://doi.org/10.1016/S0021-9258(17)32061-6
69. Sundareshwar PV, Morris JT, Koepfler EK, Fornwalt B (2003) Phosphorus Limitation of Coastal Ecosystem Processes. Science 299:563–565. https://doi.org/10.1126/science.1079100
70. Tan SZ, Prather KL (2017) Dynamic pathway regulation: recent advances and methods of construction. Curr Opin Chem Biol Mechanistic Biology * Energy 41:28–35. https://doi.org/10.1016/j.cbpa.2017.10.004
71. Tao G-B, Tian L, Pu N, Li Z-J (2022) Efficient production of poly-3-hydroxybutyrate from acetate and butyrate by halophilic bacteria *Salinivibrio* spp. TGB4 and TGB19. Int J Biol Macromol 221:1365–1372. https://doi.org/10.1016/j.ijbiomac.2022.09.141
72. Thingstad TF, Krom MD, Mantoura RFC, Flaten GAF, Groom S, Herut B, Kress N, Law CS, Pasternak A, Pitta P, Psarra S, Rassoulzadegan F, Tanaka T, Tselepides A, Wassmann P, Woodward EMS, Riser CW, Zodiatis G, Zohary T (2005) Nature of Phosphorus Limitation in the Ultraoligotrophic Eastern Mediterranean. Science 309:1068–1071. https://doi.org/10.1126/science.1112632
73. Torres-Bacete J, Luís García J, Nogales J (2021) A portable library of phosphate-depletion based synthetic promoters for customable and automata control of gene expression in bacteria. Microb Biotechnol 14:2643–2658. https://doi.org/10.1111/1751-7915.13808
74. Torriani A (1990) From cell membrane to nucleotides: The phosphate regulon in *Escherichia coli*. BioEssays 12, 371–376. https://doi.org/10.1002/bies.950120804
75. Tschirhart T, Shukla V, Kelly EE, Schultzhaus Z, NewRingeisen E, Erickson JS, Wang Z, Garcia W, Curl E, Egbert RG, Yeung E, Vora GJ (2019) Synthetic biology tools for the fast-growing marine bacterium *Vibrio natriegens*. ACS Synth Biol 8:2069–2079. https://doi.org/10.1021/acssynbio.9b00176

76. van Wegen RJ, Lee S-Y, Middelberg APJ (2001) Metabolic and kinetic analysis of poly(3-hydroxybutyrate) production by recombinant *Escherichia coli*. Biotechnol Bioeng 74:70–81. https://doi.org/10.1002/bit.1096
77. Venayak N, Raj K, Jaydeep R, Mahadevan R (2018) An Optimized Bistable Metabolic Switch To Decouple Phenotypic States during Anaerobic Fermentation. ACS Synth Biol 7:2854–2866. https://doi.org/10.1021/acssynbio.8b00284
78. Vlaeminck E, Quataert K, Uitterhaegen E, De Winter K, Soetaert WK (2022) Advanced PHB fermentation strategies with CO2-derived organic acids. J Biotechnol 343:102–109. https://doi.org/10.1016/j.jbiotec.2021.11.010
79. Wang Z, Lin B, Hervey WJ, Vora GJ (2013) Draft Genome Sequence of the Fast-Growing Marine Bacterium *Vibrio natriegens* Strain ATCC 14048. Genome Announc 1. https://doi.org/10.1128/genomea.00589-13. 10.1128/genomea.00589 – 13
80. Wei Y-H, Chen W-C, Wu H-S, Janarthanan O-M (2011) Biodegradable and Biocompatible Biomaterial, Polyhydroxybutyrate, Produced by an Indigenous *Vibrio* sp. BM-1 Isolated from Marine Environment. Mar Drugs 9:615–624. https://doi.org/10.3390/md9040615
81. Weinstock MT, Hesek ED, Wilson CM, Gibson DG (2016) *Vibrio natriegens* as a fast-growing host for molecular biology. Nat Methods 13:849–851. https://doi.org/10.1038/nmeth.3970
82. Wolfe AJ (2005) The acetate switch. Microbiol Mol Biol Rev 69:12–50. https://doi.org/10.1128/MMBR.69.1.12-50.2005
83. Wu H, Chen J, Chen G-Q (2016) Engineering the growth pattern and cell morphology for enhanced PHB production by *Escherichia coli*. Appl Microbiol Biotechnol 100:9907–9916. https://doi.org/10.1007/s00253-016-7715-1
84. Wu J, Sunda W, Boyle EA, Karl DM (2000) Phosphate Depletion in the Western North Atlantic Ocean. Science 289:759–762. https://doi.org/10.1126/science.289.5480.759
85. Ye Z, Li S, Hennigan JN, Lebeau J, Moreb EA, Wolf J, Lynch MD (2021) Two-stage dynamic deregulation of metabolism improves process robustness & scalability in engineered *E. coli*. Metab Eng 68:106–118. https://doi.org/10.1016/j.ymben.2021.09.009
86. Yévenes M, Quiroz M, Maruyama F, Jorquera M, Gajardo G (2021) *Vibrio* sp. ArtGut-C1, a polyhydroxybutyrate producer isolated from the gut of the aquaculture live diet Artemia (Crustacea). Electron J Biotechnol 49:22–28. https://doi.org/10.1016/j.ejbt.2020.10.003
87. Zhang Y, Wang M-R, Li Z-J (2026) Formate-strengthened NADH supply in *Salinivibrio* sp. TGB4 improves polyhydroxyalkanoates production. World J Microbiol Biotechnol 42:147. https://doi.org/10.1007/s11274-026-04883-4

Figures

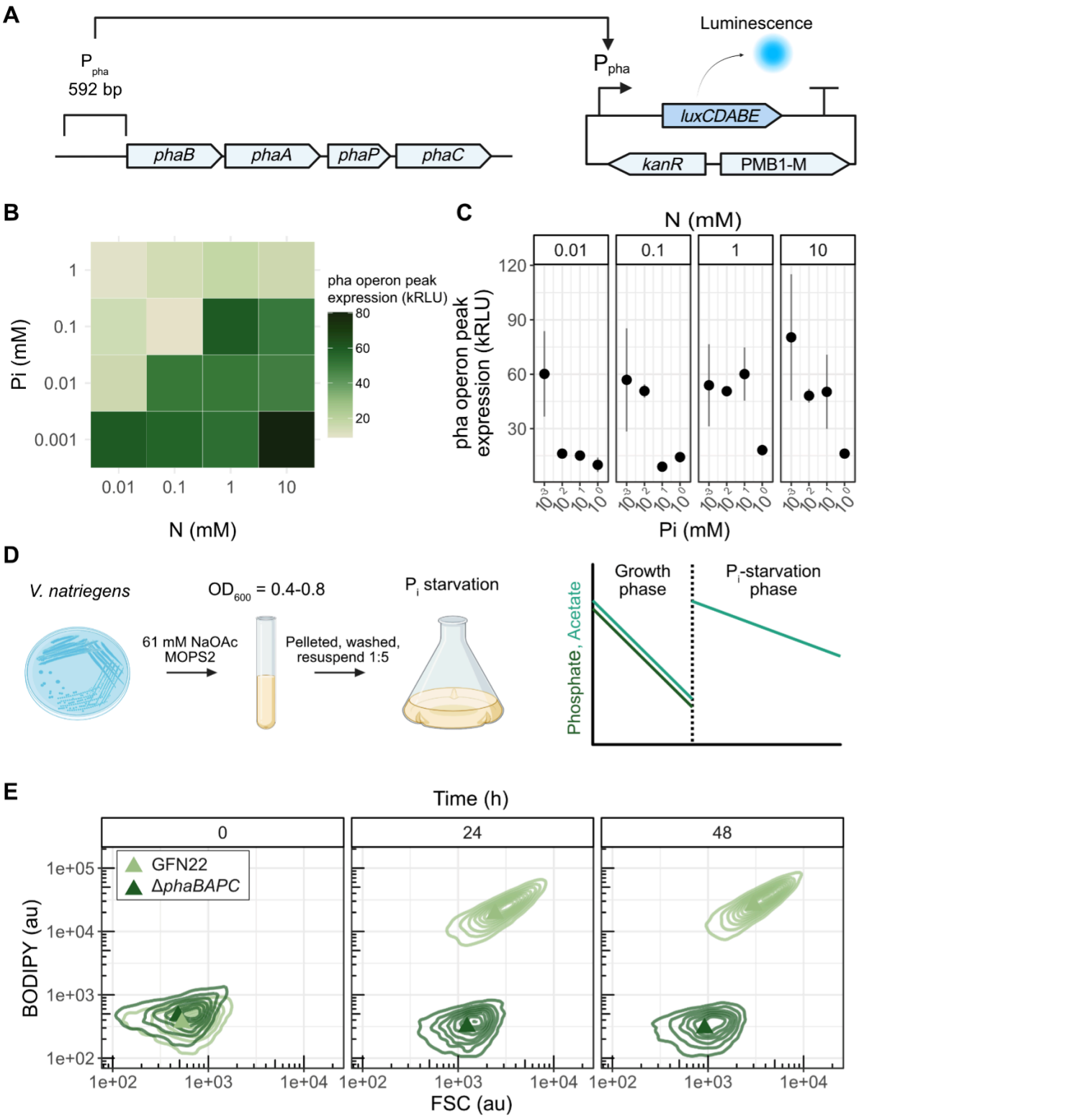


Figure 1

Phosphate, not nitrogen, induces the P_{pha} promoter and PHB synthesis in *V. natriegens*. (A) Design of the P_{pha} biosensor, in which the native P_{pha} promoter drives a *luxCDABE* luminescence operon. **(B)** Heatmap and **(C)** dot plots of the peak luminescence output of the biosensor strain (kRLU) across a matrix of phosphate and nitrogen concentrations. Cultures were grown in MOPS2 minimal medium with the indicated titrations of dibasic potassium phosphate (phosphate) and ammonium chloride (nitrogen)

from a starting OD_{600} of 0.001 in a plate reader, and the raw data were computationally shifted to start at OD_{600} = 0.01 (n = 4). **(D)** Experimental design for PHB production by phosphate starvation. **(E)** Flow-cytometric quantification of PHB accumulation by BODIPY staining in the parental strain GFN22 and the Δ*phaBAPC* control at 0, 24, and 48 h of phosphate starvation. Each symbol gives the population-mean BODIPY (intracellular PHB) and forward-scatter (FSC, a proxy for cell size) value for one strain at one timepoint.

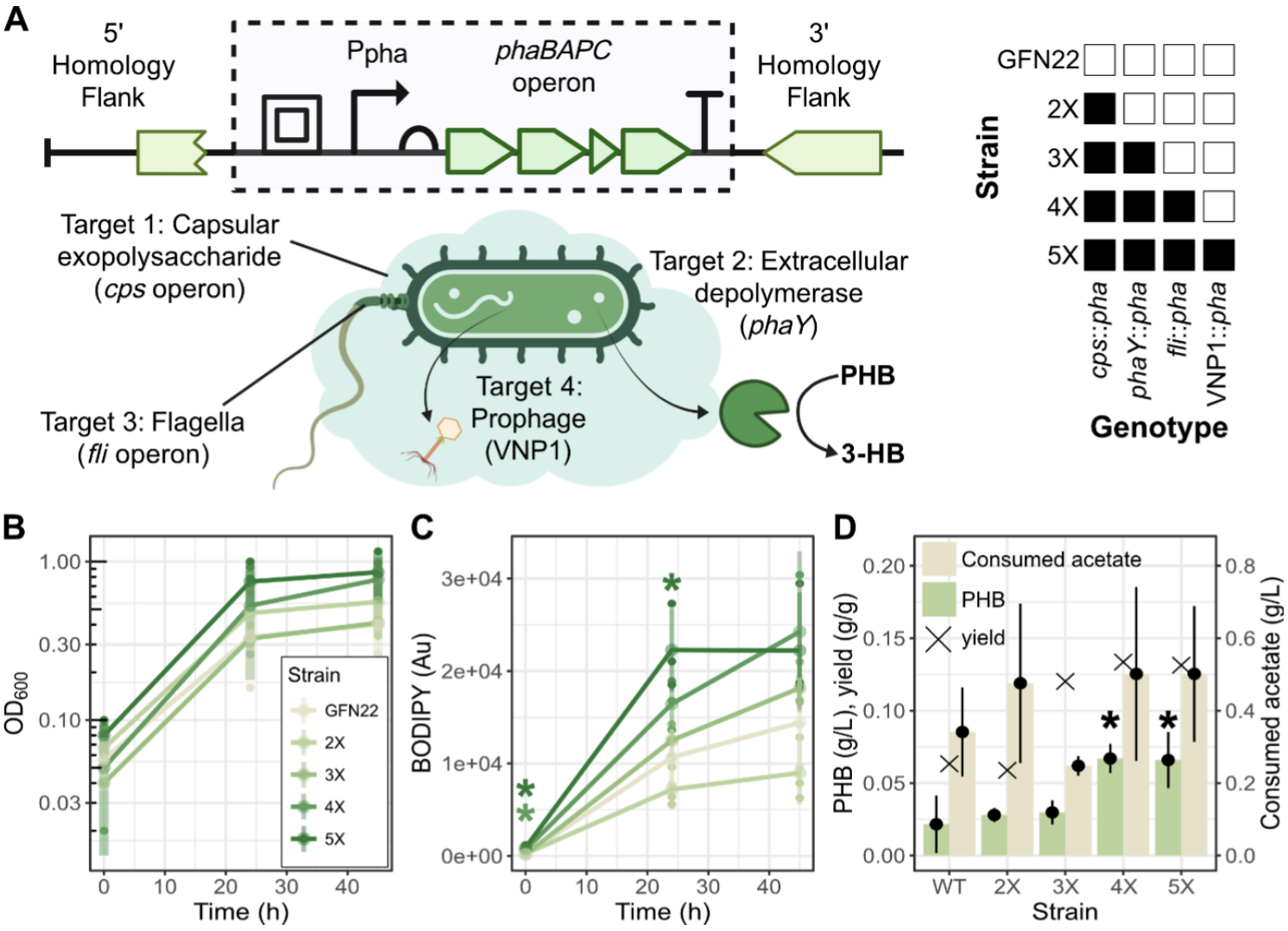


Figure 2

Effect of chromosomal copy number on the PHB titer during phosphate starvation in MOPS2 medium supplemented with 5 g/L sodium acetate (3.6 g/L acetate). (A) Diagram of integrated transcriptional unit, the targeted loci, as well as the genotype of the individual mutants. Schematic generated with Biorender. **(B)** Growth kinetics during the phosphate starvation experiment as OD_{600} (n = 3). **(C)** Intracellular PHB content as indicated by mean BODIPY values. **(D)** The amount of acetate consumed at 45 h, the resulting PHB titer and the product yield (n = 3). The yield was calculated by dividing the mean PHB titer by the mean of used acetate. Unpaired two-sample t-test was used for the statistical analysis in (B-D) using GFN22 as a reference group.

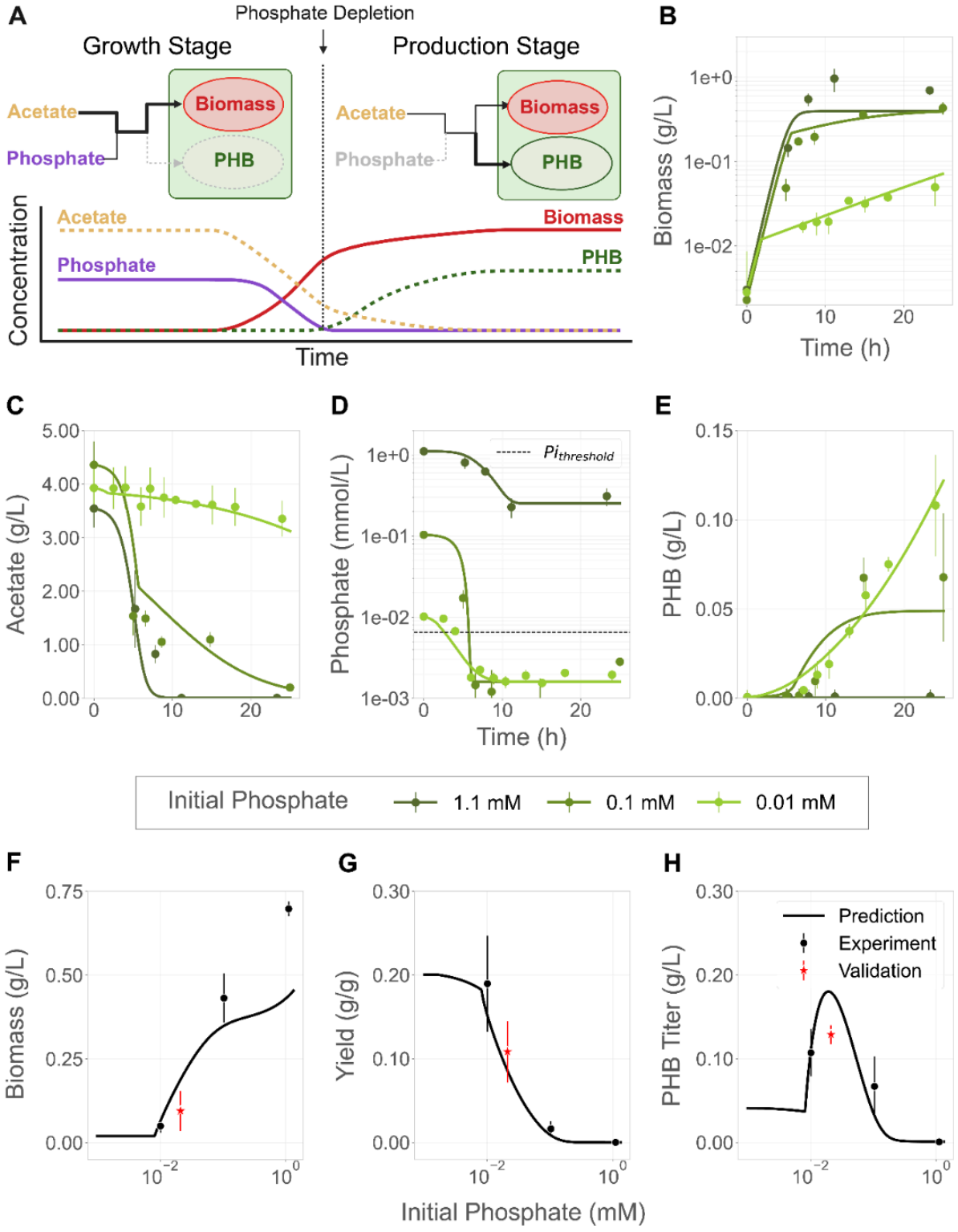


Figure 3

A kinetic model captures phosphate-controlled PHB production and predicts the optimal initial phosphate concentration. (A) Schematic of the phosphate-dependent, two-stage PHB fermentation model; arrow thickness denotes the relative magnitude of metabolic flux, and the curves beneath illustrate the predicted temporal dynamics of each metabolite. **(B–E)** Time-course kinetics of PHB production by the 5X strain at 50 mL scale in MOPS2 medium supplemented with 5 g/L sodium acetate

(NaOAc) at three initial phosphate concentrations (1.1, 0.1, and 0.01 mM). Markers denote experimental measurements (n = 3) and solid curves the corresponding model predictions. Panels show (B) biomass (log scale), (C) acetate, (D) phosphate (log scale; black dashed line, predicted $Pi_{threshold}$), and (E) PHB. (F–H) Model-predicted (F) final biomass, (G) PHB-to-acetate yield, and (H) final PHB titer as a function of initial phosphate concentration after 24 h of incubation in minimal medium. Error bars in (B–E) represent standard deviations (SD) with a 10% error floor applied for robust parameter estimation; error bars in (F–H) represent SD before application of the error floor. Simulations in (F–H) used the initial biomass and acetate concentrations of the low-phosphate group.

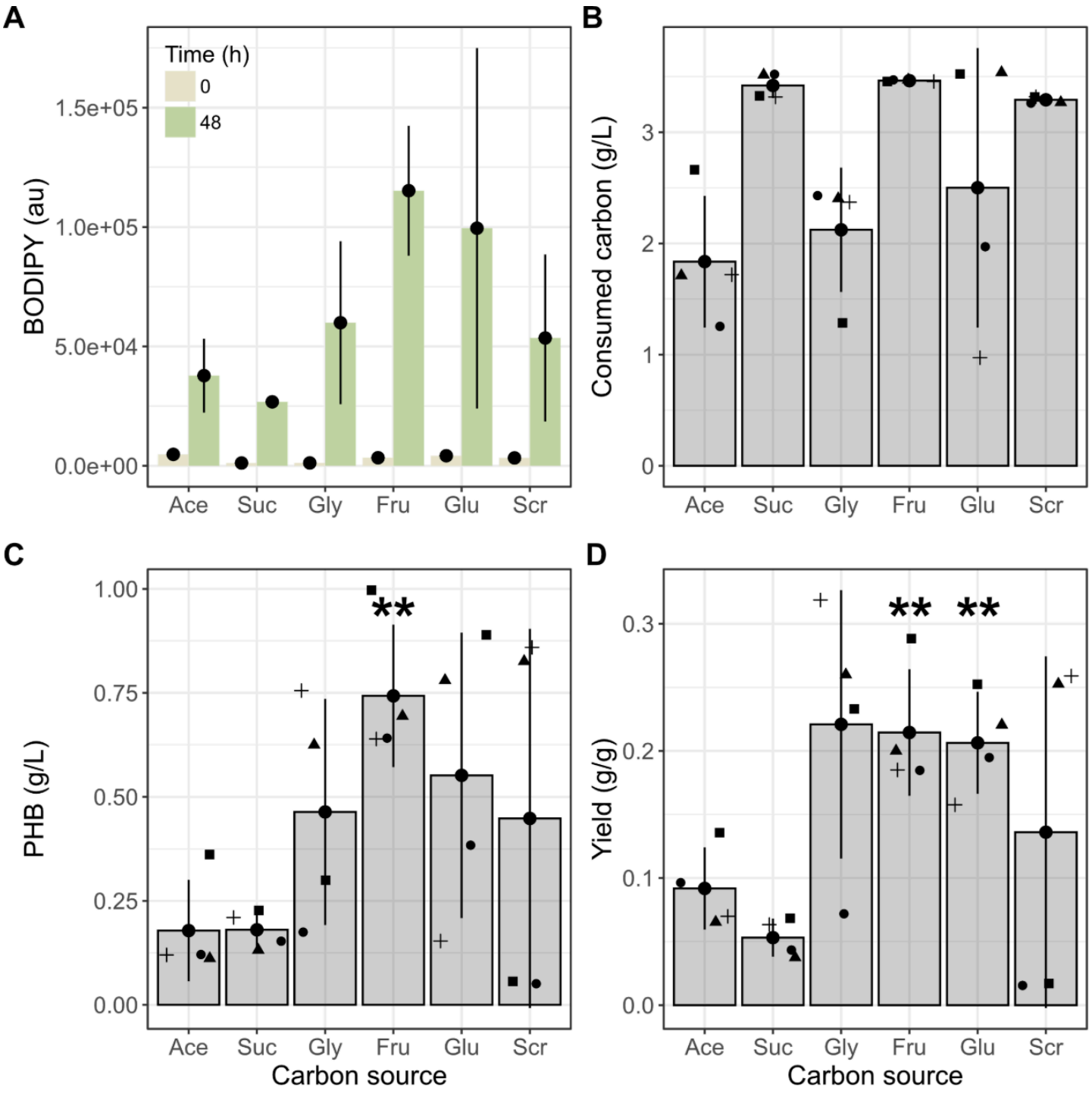


Figure 4

The effect of carbon source on PHB production via phosphate starvation from mid-exponential phase with carbon-equivalent molarity. (A) Intracellular PHB content measured as BODIPY fluorescence. **(B)** Measured carbon source that was consumed during the experiment. **(C)** Final PHB titer at 48 hours. **(D)** Measured yield by calculating PHB titer divided by the consumed carbon source of each replicate. Individual biological replicates are shown as unique shapes. The experiment was performed in biological duplicates on two different days. Unpaired two-sample t-test was used for the statistical analysis in (C-D) with acetate as the reference group. Abbreviations: Ace: acetate; Gly: glycerol; Suc: succinate; Fru: fructose; Glu: glucose; Scr: sucrose. n = 4.

Supplementary Files

This is a list of supplementary files associated with this preprint. Click to download.

- 202608Politanetal2026SupplementaryMaterial.pdf